In Situ Calibration of Hot-Film Probes Using a Collocated Sonic Anemometer: Implementation of a Neural Network

E. KIT

School of Mechanical Engineering, Tel-Aviv University, Ramat Aviv, Tel Aviv, Israel

A. CHERKASSKY

Department of Management and Control, Shenkar College, Ramat Gan, Israel

T. SANT AND H. J. S. FERNANDO

Center for Environmental Fluid Dynamics, and Department of Mechanical and Aerospace Engineering, Arizona State University, Tempe, Arizona

(Manuscript received 20 April 2009, in final form 3 August 2009)

ABSTRACT

Although the integral quantities of atmospheric turbulence are conveniently measured using sonic anemometers, obtaining relevant finescale variables such as the kinetic energy dissipation using conventional hot-film/wire techniques remains a challenge because of two main difficulties. The first difficulty is the mean wind variability, which causes violation of the requirement that mean winds have a specific alignment with the hot-film/wire probe. To circumvent this problem, a combination of collocated sonic and hot-film anemometers, with the former measuring mean winds and aligning the latter in the appropriate wind direction via an automated platform, is successfully designed and implemented. The second difficulty is the necessity of frequent and onerous calibrations akin to hot-film anemometry that lead to logistical difficulties during outdoor (field) measurements. This is addressed by employing sonic measurements to calibrate the hot films in the same combination, with the output (velocity) to input (voltage) transfer function for the hot film derived using a neural network (NN) model. The NN is trained using low-pass-filtered hot-film and sonic data taken in situ. This new hot-film calibration procedure is compared with the standard calibration method based on an external calibrator. It is inferred that the sonic-based NN method offers great potential as an alternative to laborious standard calibration techniques, particularly in the laboratory and in stable atmospheric boundary layer settings. The NN approximation technique is found to be superior to the conventionally used polynomial fitting methods when used in conjunction with unevenly spaced calibration velocity data generated by sonic anemometers.

1. Introduction

Although the integral scale quantities in the atmosphere are often measured, finescale variables (~5 cm and less) are often inferred indirectly because of measurement difficulties. Of particular importance is the rate of turbulent kinetic energy (TKE) dissipation ε, also known in atmospheric applications as the eddy dissipation rate (EDR), that underpins our understanding and nowcasting of atmospheric turbulence (Frehlich and Cornman 2002). It represents a major energy sink in the atmospheric boundary layer (ABL) and hence a mechanism of controlling energy levels at various scales (Monin and Yaglom 1971). In addition, the spatial structure of ε is used for analytical studies of atmospheric thermal convection and in computational modeling of ABL dynamics (Hunt 1984). More recently, the EDR-based techniques have been used to inform clear air turbulence for commercial aircraft as well as for optimum siting of wind turbines; hence, increasing attention is being given to understanding of the fundamental dynamics of TKE dissipation (Cornman et al. 2004; Fang et al. 2008). Traditionally, ε in the atmosphere is indirectly inferred using techniques such as fitting Kolmogorov spectral form to the measured spectra of

Corresponding author address: E. Kit, School of Mechanical Engineering, Tel-Aviv University, Ramat Aviv, Tel Aviv 69978, Israel.
E-mail: kit@eng.tau.ac.il

DOI: 10.1175/2009JTECHA1320.1

sonic anemometers (Kaimal and Finnigan 1994), which is also known as the inertial dissipation technique, or by employing special retrieval techniques to low-resolution lidar or radar measurements based on assumed theoretical spectral shapes (Frehlich and Cornman 2002). Such techniques also assume that turbulence is statistical stationary, which is not always satisfied in the atmosphere. The direct measurement of ε in the atmosphere using high-resolution instruments, such as hot film/wire, that can resolve dissipation scales has been rare (Skelly et al. 2002; Poulos et al. 2006), given the intricacy and logistical restrictions of the instruments involved. Standard hot-film/wire techniques work on the premise that the change of resistance (or an equivalent voltage change) produced in a heated wire resulting from cooling of a passing flow is a function of velocity. Thus, a reliable calibration procedure is necessary to convert the voltage to velocity. This procedure becomes more complicated for two-dimensional (2D) or 3D probes, wherein the wires are inclined to the flow direction.

The approximation of input–output relationships, or transfer function, for hot-wire/film calibration is usually realized by measuring the voltage outputs for a range of flow velocities in low-turbulence environments. The flow velocity (and if required the flow direction) is systematically changed over a parameter range of interest, thus obtaining input points separated at regular intervals. Obtaining such calibration curves in the atmosphere has been a bane, given the difficulty of working in unfriendly outdoor environments and the necessity of frequent calibrations in view of slowly changing probe performance resulting from contamination.

Hot films/wires have been recently used in field experiments together with sonic anemometers, and attempts have been made to use suitably processed data from the latter to build a calibration set for the former. During the Cooperative Atmospheric Surface Exchange Study (CASES-99) in October 1999, Skelly et al. (2002) deployed two levels of triple-hot-film and sonic anemometers on a 5.5-m tower. Each hot film was collocated 5 cm from the sonic sensing path on a common boom. According to the authors, seven constant-temperature triple-hot-film anemometers were calibrated prior to the deployment using the procedure of Miller et al. (1989), where a laboratory free-jet wind nozzle was used as the controlled velocity source (calibrator). Each hot-film sensor was mounted perpendicular to the flow in the potential core of the jet, adjoining a Pitot tube, to obtain an effective cooling velocity V_{ei}. In the outdoors, the data were taken only when the winds were from a particular direction, thus avoiding complexities of directional dependence. The change of calibration over the experiment was said to be minor; thus, the calibration obtained prior to the experiment was used. Our experience, however, suggests that calibrations of multiple hot-film/wire probes are short lived and calibrations for different wires diverges significantly with time. Figure 2 of Skelly et al. (2002) indeed indicates a probe drift over the experimental period, suggesting the necessity of frequent calibration.

A similar setup to that of Skelly et al. (2002) has been deployed in the Terrain-Induced Rotors Experiment (T-REX) in Owens Valley, California, during March–April 2006. The system was dubbed the Outdoor Three-Dimensional In-Situ Calibrated Hot-film Anemometry System (OTIHS). An in situ calibration method was suggested for OTIHS based on the first-use data obtained from simultaneous measurement of collocated sonic and hot-film anemometers, with the former providing velocity data for calibration of the latter (Poulos et al. 2006). The hot film was aligned with the prevailing wind direction measured by the sonic anemometer using an automated platform. The data processing for T-REX work is still in progress, and the calibration approach the OTIHS developers anticipate to use will be built upon those of van Dijk and Nieuwstadt (2004a,b), in particular the lookup table approach of van Dijk and Nieuwstadt (2004b). In the latter method, a set of calibration samples $E_{cal,I}$ is first collected; for a number of absolute velocities (with arbitrary intervals), a set of orientations with regular angular intervals is acquired. In other words, the lookup table method requires calibration over regular angular intervals, which is unachievable with an in situ calibration method based on a random dataset from sonic anemometers. These data are unevenly spaced in the data domain, for which the applicability of standard interpolation techniques such as the polynomial least squares fitting (PF) for producing calibration approximations is in doubt.

Considering the versatility of the OTIHS concept, in that it opens up the possibility of using hot films/wires in the field without cumbersome calibration devises, the present authors decided to investigate possible approximation techniques for accurate interpolation of velocity–voltage data, even in the presence of unevenly distributed calibration data. During this research, the neural network (NN) approach (e.g., Haykin 1998) emerged as a strikingly successful method, and its application for hot-film calibration is the main topic of this paper. An NN is a computational device that produces appropriate outputs from inputs, based on a selected architecture and subsequent training to perform intended tasks. If the general relationships are mapped as functions, say from Rn to Rm, then an NN with smooth activation functions can approximate continuous functions with compact support (i.e., all continuous functions whose domains are

closed and bounded in Rn). This property is a result of the Stone–Weierstrass theorem: all continuous functions with compact support can be approximated to any degree of accuracy by a neural network of one hidden layer with a sigmoid or hyperbolic tangent activation function (Nguyen et al. 2003; Haykin 1998). It is this property that we wish to exploit for calibrating hot films/wires with uneven distributions of datasets. In this paper, the following methodology was adopted:

1) A laboratory jet device (calibration unit or calibrator) was used to obtain an evenly distributed calibration dataset [called the calibrator-based set (CBS)] by placing the hot film in the potential core of the jet, with a miniature Pitot tube alongside for velocity measurement. The voltage–velocity calibration was realized using (i) the PF and (ii) training of an NN. This jet device was used both in the laboratory and field experiments for obtaining CBS.
2) The hot film was then placed within the probe volume of a sonic anemometer, and the combination was used for the measurements at different far field sections of the laboratory jet where the flow is turbulent as well as in the field to measure atmospheric turbulence. The utility of these datasets are twofold: to generate a calibration dataset [called the sonic-based calibration dataset (SBS)] and to use the same dataset to compute high-resolution turbulent velocity fields for hot films. The SBS was used to determine the coefficients of a PF and to train the NN, as in CBS.

Table 1 lists the datasets and calibration procedures used for all four cases. For the CBS, the interpolations based on NN and PF were found to be essentially identical, implying that both NN and PF work equally well. For SBS, however, the NN performed equally well as the CBS case, but the calibration with PF was found to be unacceptable. Note that the CBS-based PF calibration (CBS-PF) can be construed as the baseline (reference) for comparison, because it is the standard calibration procedure. Although not as good as for the laboratory case, the NN calibration (SBS-NN) was found to be in agreement with the standard CBS-PF at least under certain atmospheric conditions. SBS-PF was found to be unacceptable for outdoor (field) calibration.

TABLE 1. A list of datasets and calibration procedures used and nomenclature.

Calibration datasets/ approximations	PF	NN
CBS	CBS-PF (1)	CBS-NN (2)
SBS	SBS-PF (3)	SBS-NN (4)

2. Experimental methodology

In this section, the jet facility used for the multiple purposes of calibration (at the nozzle) and as a canonical turbulent flow (downstream) in the laboratory and as a calibrator in the field is discussed first. The mean jet direction and velocity are known and temperature variations are minimal in the laboratory, whereas in the field the wind velocity and direction are variable, with convection (strong vertical velocity and temperature fluctuations) being the rule rather than the exception during the day. Our objective is to evaluate the feasibility of a NN to calibrate hot-film probes using in situ velocity vectors from a sonic probe in the field (under different ABL conditions) or laboratory.

a. Calibration facility

The custom-made calibration unit consisted of a computer controlled blower, connected to a settling chamber followed by a contraction with a cross-sectional ratio of approximately 11 (Fig. 1a) and exit nozzle diameter $D_e = 38.1$ mm. The same facility was used to measure all three components of turbulent velocity at various downstream cross sections.

The design of the probe assembly enabled rotation of the probe in yaw direction (Fig. 1b) with the yaw-angle adjustment automated using a National Instruments model PCI-7330 motion control board and a US Digital model MD2S microstepping motor (5 microsteps per step) driver. The yaw angle in this design could be varied over a wide range ($\pm 90°$) while the probe tips fixed in space. A National Electrical Manufacturers Association (NEMA) size 17, 200-step (1.8°) stepping motor and 15:1 ratio planetary gearbox (Lin Engineering type 4218S-02-PG15) was used to rotate the assembly, resulting in a very high angular resolution of 0.024° per step. Stepper motor and control board were interfaced using a National Instruments UMA-7764 Universal Motion Interface.

b. Instrumentation

Two orthogonal end-flow X probes (TSI model 1241–20W; see Fig. 1d), which are commonly used in water applications, were selected considering their robustness compared to hot wires; probe ruggedness is imperative in field applications where vibrations and airborne particulates are common. Fine-wire probes provide a faster time response, but this was not required to capture flow dynamics in the present case. The 1241–20Ws are platinum film probes with a sensing diameter of 50.8 μm and a sensing length of 1.02 mm (which defines its

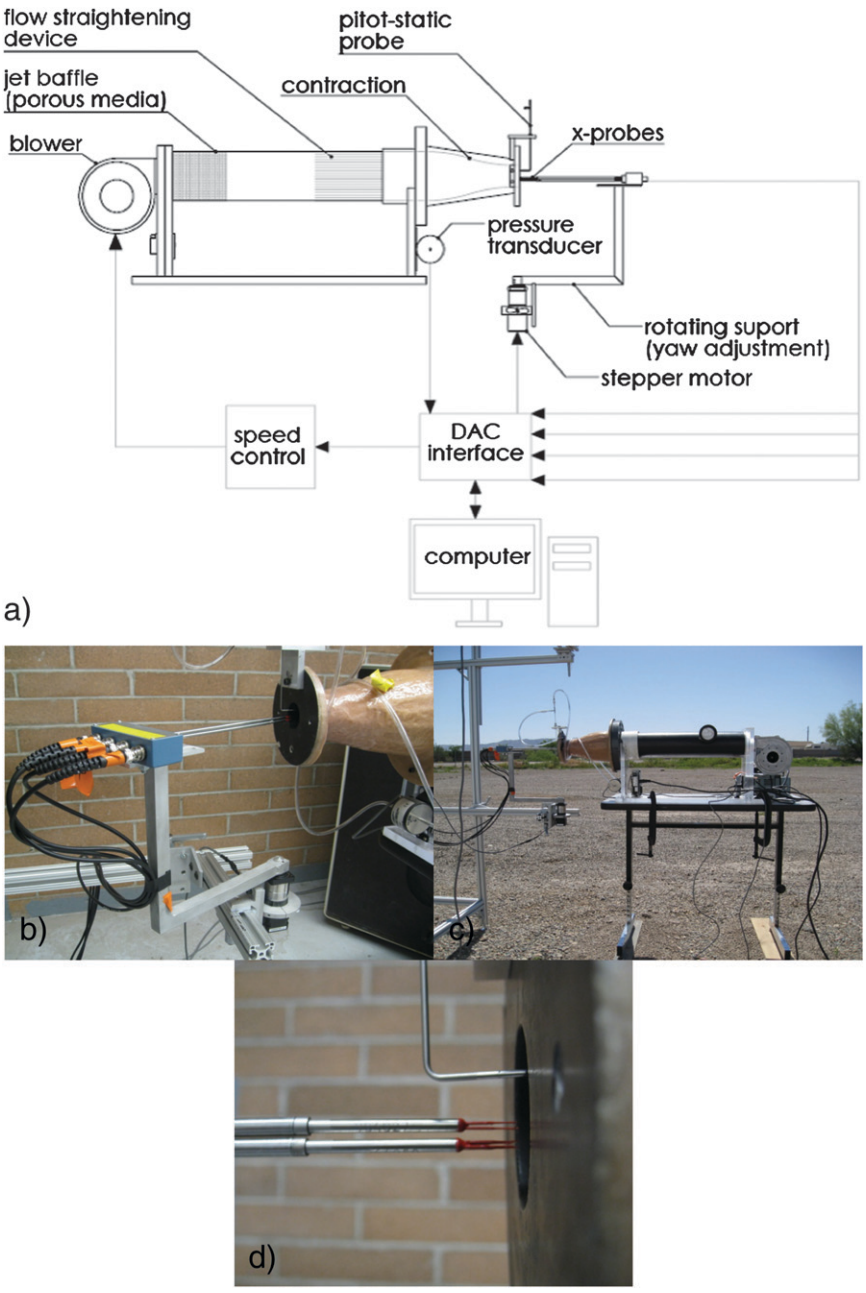

FIG. 1. Calibration setup: (a) calibration facility, (b) schematic of calibration unit, (c) calibration unit deployed in the field, and (d) a close-up of miniature Pitot tube and two X hot-film probes.

spacial resolution). The sensor orientation is 45° relative to the connector end of probe. Two dual-sensor probe supports were modified from their original 36″ length to 8″ and were mounted vertically stacked (in the same vertical plane), with an overall spatial resolution better than 6 mm (limited because of the size of the probe support). A collar was fabricated for the probe supports, permitting rotation of each probe. Both X probes were oriented in the horizontal plane during calibration, and thereafter the upper probe holder was rotated to obtain two orthogonal X probes, thus providing a convenient way to measure all three velocity components with 2D probes. In this case, the out-of-plane velocity components need to be small, thus imposing a constraint on the type of velocity field the probe combination can measure.

The anemometer system employed was the Dantec type 56C01 with constant-temperature anemometer (CTA) 56C17 bridges. Signal conditioning was provided in part by using standard Dantec-made auxiliary boards and in part by using type 3202 Krohn-Hite low-pass filters. The ultrasonic anemometers used were of the type R. M. Young, model 81000 (see R. M. Young Company 2001). The velocity measurement range was set from 0 to 10 m s^{-1} with a sampling frequency of 32 Hz (maximum allowed). These anemometers provide all three velocity components with a relatively low spatial (~10 cm) and temporal (~16 Hz) resolution, and they are a common workhorse in the field.

c. Laboratory experimental procedure

All experiments were conducted with a nozzle exit velocity ~8 m s^{-1}, measurements were taken at L = 2000, 3000, and 4000 mm, and the temperature variation during the experiments was insignificant (less than a few tenths of a degree). Both CBS and SBS were used in data analysis. First, a CBS was obtained at the nozzle exit, followed by turbulent velocity measurements at L = 3000 mm. The second calibration dataset, SBS, was obtained by low-pass filtering (via data averaging) the simultaneously measured voltage signal of hot film and the velocities of sonic. With sampling frequency of 1000 Hz and the experimental duration of 300 s, 300 000 data points were obtained, which is adequate for any statistical analysis. The internal maximum sampling frequency of Sonics is 32 Hz, but 1000 Hz was used for sonic data acquisition (DAQ) to simplify the procedure and subsequent analysis.

To obtain the SBS, the data points were averaged over 0.3 s, yielding a dataset of 1000 points. To apply NN, this calibration dataset served as a training dataset, and 1000 points is an appropriate number for a training dataset, even when the data points are unevenly distributed. With orderly distributed data, as in CBS, a fewer number of points are acceptable. In few laboratory experiments, both the polynomial coefficients for PF and the model parameters for NN were obtained for CBS, which contains only 77 points. Nevertheless, as will be shown later, this limited number of points was sufficient for successful NN training.

Note that although the probe combination enables measure all three components of velocity, its calibration was performed by varying the yaw angle of both X hot films (oriented in the horizontal plane) relative to the flow. This 2D calibration differs from the 3D calibration of a four-wire 3D probe described in Tsinober et al. (1992) and van Dijk and Nieuwstadt (2004b). Note that CBS-PF represents the standard method of calibration (Tsinober et al. 1992; Gulitski et al. 2007a,b,c; van Dijk and Nieuwstadt 2004a,b; Dobbeling et al. 1990, 1992), although somewhat different techniques based on effective velocity approach are also being used (Balint et al. 1987, 1988, 1991; Jorgensen 1971; Kit et al. 1987, 1988; van Dijk and Nieuwstadt 2004b).

For calibration purposes, a lookup table method can be applied. For example, van Dijk and Nieuwstadt (2004b) suggested the following procedure: (i) collect a set of calibration samples $E_{\mathrm{cal,I}}$; (ii) for a number of absolute velocities (with arbitrary intervals), scan a set of orientations with regular angular intervals. The number of calibration samples required to get the desired accuracy in their case was 16 250 for the classic probe (angular increments of 3° and uniform velocity increment of 0.28 m s^{-1}), which may take an entire day. This is inconvenient in practice and untenable in field situations. In addition, in atmospheric flows, hot-film measurements face many additional problems over a day, such as aging, contamination, and calibration drift. Other issues of concern include path averaging of signal over the wire, nonuniform temperature distribution over the wire, loosely mounted wires, thermal cross talking, electrical cross talk between the wire signals, and decorrelation of signals resulting from short wire separation.

d. Field experimental procedure

In the field, obtaining CBS followed the same procedure as in the laboratory. Thereafter, the hot-film probe was collocated with the sonic anemometer and the combination was installed on a tower, with provisions for changing its height from 1 to 3 m above ground level. The generation of the calibration dataset (SBS) followed the same steps as that in the laboratory, except that the data taken in atmospheric turbulence were used.

e. Data acquisition and calibration details

DAQ was accomplished using a National Instruments data acquisition board, model PCI-6024E. The software-selectable board gain was set to ±5 V. The board resolution is 12 bit with a maximum sampling rate of 200 000 samples per second. A 16-channel (8 differential) analog input and 2-channel analog output were used for laboratory data acquisition. During the calibration, signals from two X probes (4 channels), a pressure transducer, and the temperature from the sonic anemometer were acquired. In field measurements, 13 channels were used: 4 channels for each sonic anemometer, 4 for the X probes, and 1 for the pressure transducer signal (during calibration). Sampling was performed at 1000 Hz in the laboratory and at 2000 Hz in most field experiments.

During the calibration, both X probes were oriented in the horizontal plane and placed at the nozzle exit in the potential core of the jet (low turbulence intensity)

alongside a miniature Pitot-static probe. The Pitot tube provided simultaneous velocity measurements via a high-resolution Baratron-type pressure transducer. The velocity field at the nozzle exit was of high spatial homogeneity, allowing simultaneous calibration of both X probes. The calibration procedure was fully automated, and the data acquisition, stepper motor (to change the probe yaw angle), and blower were controlled by the same computer. A full calibration dataset (CBS) consisted of 11 yaw positions (from ±30°) at 7 variable velocities.

As mentioned, two types of turbulent flows were investigated: laboratory turbulent jet and lower atmospheric boundary layer flow. In the former, axially developing turbulent jet emanating from the calibrator, sufficiently away from the nozzle, was used. Measurements were made using collocated sonic and hot films; thus, the homogeneity of the velocity field over the probe combination was imperative. The Pitot tube and hot-film measurements showed that such is achieved at distances of $L > 2000$ mm ($94.5D_e$), where the streamwise component was homogeneous over the sonic probe volume (the effective sonic diameter $D_s = 100$ mm) within 10%. Most laboratory measurements were conducted at the $L = 3000$ mm cross section, but a few were also performed at $L = 2000$ mm to elucidate the effects of higher turbulence intensities and $L = 4000$ mm for low turbulence intensities.

Unlike in the laboratory, the direction of atmospheric flows is variable, but the current facility offered the advantage of following the mean flow direction in the field by employing the same stepper motor and rotating frame that was used for calibration. Therein, a feedback signal was derived based on the three velocity components measured by the sonic, which were interrogated at every 60-s interval. In doing so, the signals were averaged over the last 5 s of each 60-s record to allow sufficient time to filter out smaller-scale fluctuations caused by the variability of wind direction. If the directional variability between the beginning and the end of a 60-s record is more than 10° different, the record was discarded in data processing.

As described previously, the probe calibration was made in the plane of the probe only, requiring the out-of-plane velocity component to be relatively small. These requirements are automatically fulfilled for a horizontally oriented X hot film, because the mean vertical velocity in the lower ABL is usually small and only the fluctuating normal velocity is dominant. When the X-film probes are vertically oriented, however, the wind velocity should coincide with the probe plane, which represents a constraint in data processing. The effective velocity approach widely used for calibration indicates that the errors become noticeable when the out-of-plane velocity exceeds 10% of the mean velocity value, and this constraint was imposed during data processing.

In generating the SBS, the following should be borne in mind:

1) Although the resolutions of two instruments are significantly different, at low frequencies the velocity fields sensed by both probes are the same, and hence both ought to yield the same velocity field upon low-pass filtering. The calibration dataset SBS can be built using low-pass-filtered signals of sonic anemometer (velocity) and hot-film bridges (voltage).
2) A drawback of the last approach is the nonlinearity of heat transfer (the latter underpins the principle of hot-film operation). Owing to this nonlinearity, a part of the high-frequency signal of the anemometer bridge output is contributed by the low-frequency velocity field. The low-pass filtering will filter out this high-frequency contribution, although it is produced by the low-frequency part of velocity spectrum. It is difficult to estimate this loss, although the loss should increase with the turbulent intensity. This paper intends to investigate (i) the efficacy of using SBS in calibrating hot films compared to the standard calibration procedure (CBS), (ii) conditions under which SBS is sound, and (iii) whether special techniques can be used to make SBS and CBS closely compatible. Because the difficulty of in situ calibration is the bane of field deployment of hot films, a reliable SBS will offer a breakthrough in atmospheric sensing.

As discussed, CBS and SBS methods were used in conjunction with PF and NN models to determine the output (variable velocity components felt by the hot-films probes) and input (voltages generated by the CTA across the wires) relations for each of the hot films. In the PF case, commonly used polynomial expressions were employed. The successful use of PF approach for X wires was recently reported in Kit et al. (2005, 2007), where a least squares fit by fourth-order polynomials was used to compute 15 polynomial coefficients for each velocity component.

The polynomial approximation has the following form [van Dijk and Nieuwstadt (2004a,b)]:

$$U_i = f_i(E_1, E_2) \quad \text{and}$$

$$f_i(E_1, E_2) = \sum_{kl} c_{ikl} P_k(E_1) P_l(E_2);$$

$$P_k(E) = E^k, \quad 0 \le k, \quad l \le 4, \quad k + l \le 4;$$

the coefficients of this expression are calculated by solving a system of linear equations.

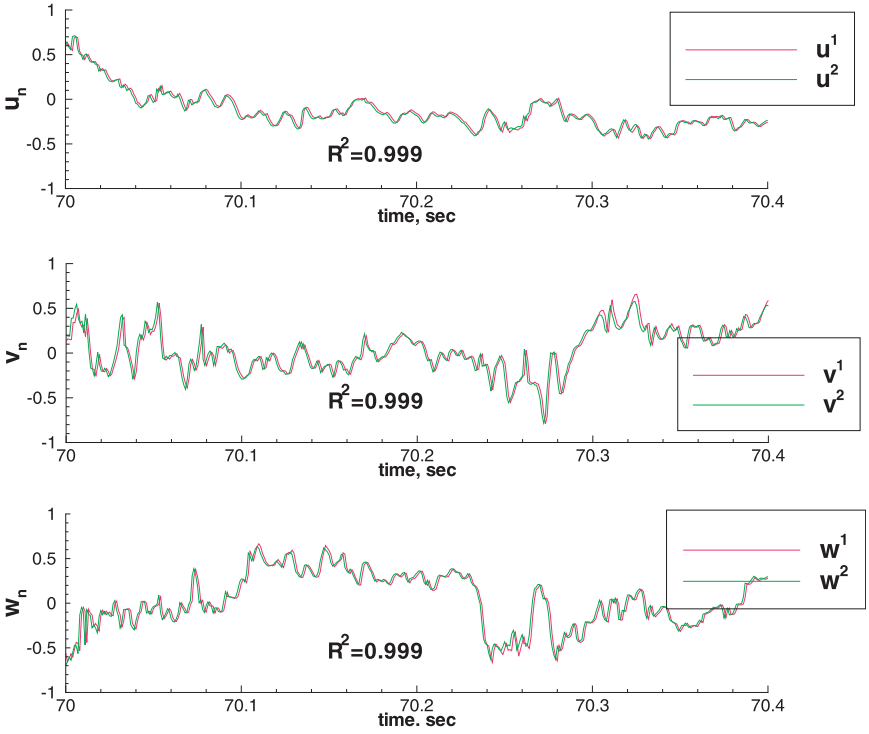

FIG. 2. Plots of (top) streamwise, (middle) transverse, and (bottom) vertical normalized velocity component for Lab_Expt 1, where $L = 3$ m. Red plot shows CBS-PF, and green plot shows CBS-NN. For superscripts, see Table 1.

The same set of calibration data is used to approximate the input–output relations by applying an NN approach, a detailed description of which is given in the appendix. The neural network approach has been previously applied on a limited basis (Al-Salaymeh and Ashhab 2006, 2007) for hot-wire/film calibration, but such work has been confined to single hot-wire sensors under different air densities.

3. Laboratory experimental results

The time series of three velocity components were computed for the entire dataset measured in Lab_Expt 1 using both approaches, PF and NN trained, with CBS, and a typical comparison is shown in Fig. 2. The data represent fluctuations after subtraction of mean velocities and normalized by respective 3 times RMS values. Green corresponds to velocity components computed using reference (CBS-PF) calibration, and red represents those based on CBS-NN model. The agreement is excellent, with the correlation coefficient higher than 0.99, for all three velocity components. The fact that the two very different calibration procedures yield practically the same result indicates that both models are appropriate for carrying out calibration of this probe system.

A comparison of two time series of normalized streamwise, spanwise, and vertical velocities measured at the jet axis by the hot films, computed using CBS-PF and SBS-NN for the same laboratory experiment, is shown in Fig. 3. Green corresponds to velocity components computed using reference (CBS-PF) calibration, and red represents those based on SBS-NN model. The results summarized in Table 2 clearly show that, even at relatively high turbulent intensities (>25%), the NN approach for calibration yields results close to those obtained using the reference method (CBS-PF).

In Fig. 4, the results are presented for $L = 2000$ mm, wherein the turbulence intensity is higher (by about 30%) than in the previous example. Although the flow in the sonic probe volume is somewhat inhomogeneous because of shorter distance from the jet exit, the NN model yields results in par with those obtained using the reference method.

The same PF method can be used with SBS, but this calibration set differs from CBS in that the latter is constructed using data obtained at regular intervals covering the entire range of hot-film measurements. Conversely, the SBS data are unevenly distributed over an uncontrolled range of velocities for each velocity component. A comparison of velocity fields obtained using

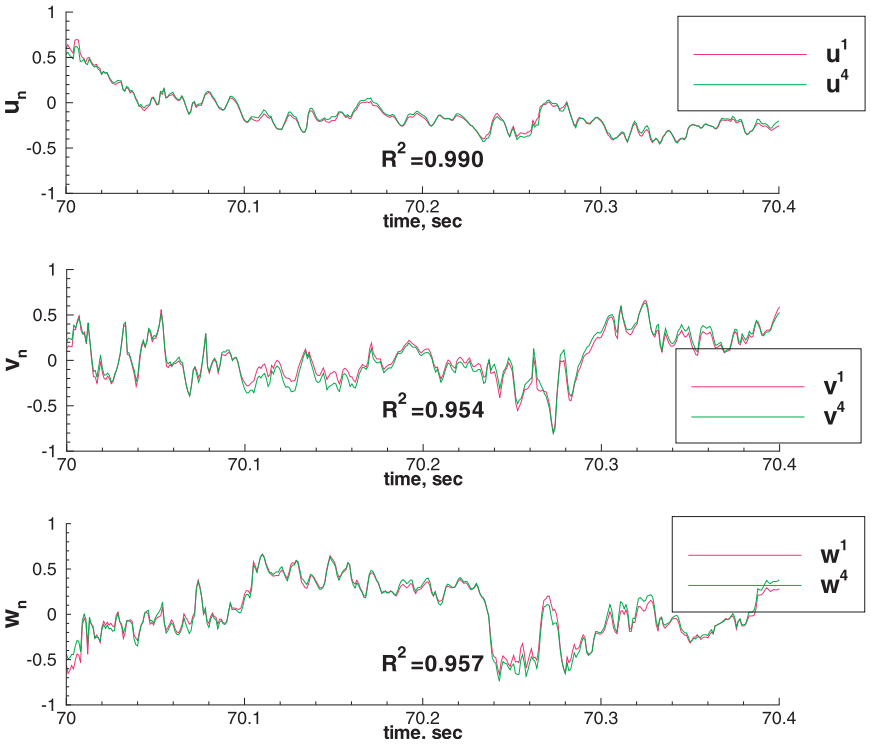

FIG. 3. As in Fig. 2, but green plot shows SBS-NN.

SBS-PF with that of the reference (CBS-PF) method is presented in Fig. 5.

The agreement is poor, and this is true for other similar comparisons (not shown here). Therefore, the use of PF with SBS is not recommended. The success of NN when used with SBS can be attributed to its intrinsic feature, discussed in section 1, with regard to functions with compact support.

It can therefore be concluded that, under controlled laboratory conditions, the NN approach is a highly suitable method for calibrating hot films. High turbulent intensities have only weak deteriorating effects on the quality of results obtained using CBS-NN or SBS-NN when compared to the reference method (CBC-PF), as explained previously, based on Fig. 4.

4. Field experimental results

In contrast to controlled laboratory conditions, the wind direction and speed under field conditions have

TABLE 2. Normalized mean and RMS (σ) velocities based on different techniques.

Expt	Dataset/calibration method	Velocities					
		u_0 (m s^{-1})	v_0/u_0	w_0/u_0	σ_u/u_0	σ_v/u_0	σ_w/u_0
Laboratory jet experiments							
Lab_Expt 1, L = 3 m	CBS-PF	2.20	0.0236	−0.0050	0.257	0.207	0.200
	CBS-NN	2.20	0.0477	−0.0077	0.252	0.210	0.207
	SBS-NN	2.20	0.0245	−0.0036	0.264	0.209	0.200
	SBS-PF	2.18	−0.0812	−0.0839	0.411	0.369	0.532
Lab_Expt 2, L = 2 m	CBS-PF	3.1	0.0161	−0.0387	0.293	0.203	0.210
	SBS-NN	2.66	0.0684	−0.0248	0.286	0.187	0.178
Field experiments							
Field_Expt 1, 1400–1500 30 Mar 2008	CBS-PF	3.347	0.239	0.0024	0.401	0.286	0.195
	SBS-NN	2.271	0.539	0.0097	0.498	0.581	0.271
Field_Expt 2, 0530–0630 6 Apr 2008	CBS-PF	1.47	0.0680	−0.0551	0.211	0.191	0.184
	SBS-NN	1.247	0.0537	0.0305	0.248	0.204	0.192

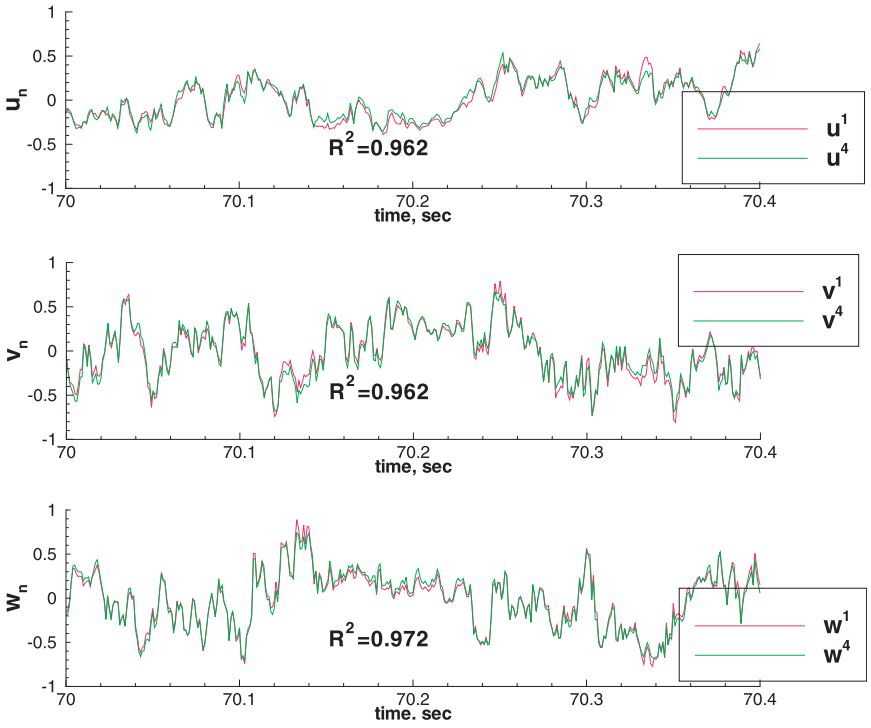

FIG. 4. As in Fig. 2, but for Lab_Expt 2, $L = 2$ m, and green plot shows SBS-NN.

significant variability, including diurnal thermal forcing that produces convective boundary layer (CBL) during the day and stable boundary layer (SBL) at night. The former consists of turbulent convection that produces rising and falling thermals over the entire boundary layer and shear-produced (mechanical) turbulence near the ground, whereas the latter inhibits turbulence and confines it to intermittent patchy regions or maintains weak turbulence over the entire boundary layer (Monti et al. 2002; Pardyjak et al. 2002). Considering all, it can be expected that the NN will provide better results for the SBL. As mentioned, the measurement issues akin to wind variability were addressed using an automated wind direction tracking system, and experiments were conducted covering the entire diurnal cycle. The parameters corresponding to the field experiments are given in Table 2.

Figures 6 and 7 show the measurements carried out on 30 March and 5 April 2008, respectively. It can be seen from Fig. 6 (Field_Expt 1) that, even under strong convection, there are periods where the results obtained by the reference (CBS-PF) and SBS-NN are in reasonable agreement. As shown in Fig. 6b, however, significant differences in the results were noted when there are strong bursts. Further analysis is necessary to determine criteria to delineate conditions for acceptable data from those unreliable, which appear to occur during convection events (this, in part, can be attributed to the strong vertical velocities present during convection, which makes the present calibration procedure unsuitable). The results of an experiments conducted during nocturnal period (Field_Expt 2) are presented in Fig. 7, which show a good agreement between results obtained using SBS-NN and CBS-PF calibrations. The quality of agreement is almost as good as that obtained under controlled experiments in the laboratory.

5. Spectral measurements

The spectra computed using data processed using CBS-PF and SBS-NN procedures are presented in Figs. 8–11. They show the well known $-5/3$ slope at lower frequencies and a faster decay at larger frequencies. Although their behaviors are very clear and consistent in the laboratory jet experiment (Figs. 8, 9), the field experiment performed throughout the night shows an interesting bump in the slope, including even a change of sign sometimes, at frequencies ~50–100 Hz (see Fig. 11). This phenomenon remains unexplained and is in need of further study.

The spectra obtained using data from sonic are presented in Fig. 12. Note that the sampling rates used for sonic and hot films were the same. Consequently, the spectra beyond 16 Hz are unphysical and represent

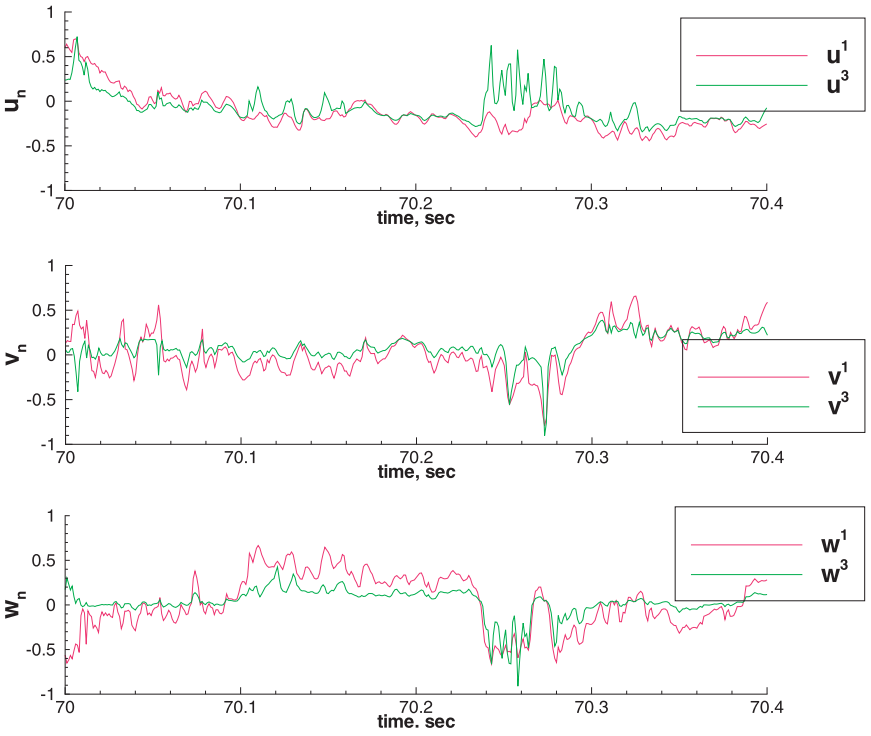

FIG. 5. As in Fig. 2, but green plot shows SBS-PF.

noise. When compared with Fig. 11b, the spectra in Fig. 12 show similar values at frequencies below 16 Hz, but as expected at higher frequencies they deviate substantially.

6. An example from NCAR data

The National Center for Atmospheric Research (NCAR) group has kindly provided us a sample of their unpublished (raw) data from the OTIHS system taken during the T-REX experiment. Note that the reference CBS-PF does not exist for this dataset. We, however, employed these data to verify the utility of the NN method proposed here by calculating canonical turbulent quantities and inspecting their trends. Based on section 4, nocturnal data taken under stably stratified and low-turbulence conditions in general are expected to have higher reliability than daytime data; hence, a 300-s-long piece of data taken at night was processed using SBS-NN. The results are shown in Fig. 13.

In Table 3, an analysis of their data is presented to illustrate that the NN method gives plausible results, such as negative Reynolds stress in the streamwise vertical plane. Other Reynolds stresses are close to zero. It is interesting that the voltages across different wires of the multihot-film probe are strongly correlated, and it is the NN procedure that, using these voltages as an input, generates output velocity vectors that behave differently. As noted above, in these experiments, an independent calibration is absent and correctness of the NN calibration procedure can be only deduced from circumstantial evidence, particularly the negative Reynolds stress $\overline{uw}$ and vanishingly small other stresses, as was obtained in these experiments (Table 3).

The spectra of u, v, and w are presented in Fig. 14. The spectra show $-5/3$ slope but only at relatively low frequencies. At higher frequencies, the decay becomes significant and the spectral plots diverge from the typical inertial range slope.

7. Conclusions

The present study dealt with the feasibility of using a neural network (NN) to calibrate hot-film probes of a system of instruments, wherein hot-film probes are collocated with a sonic anemometer (sonic) and data from both are acquired and processed simultaneously. Note that, in this case, the NN model is used for obtaining an in situ velocity–voltage transfer function for calibration rather than for any predictive purpose (which is the celebrated application of NNs). Sonics are commonly used in atmospheric research, but because of their low space–time resolution, the utility in obtaining information on finescale turbulence is limited. Hot-film/wire

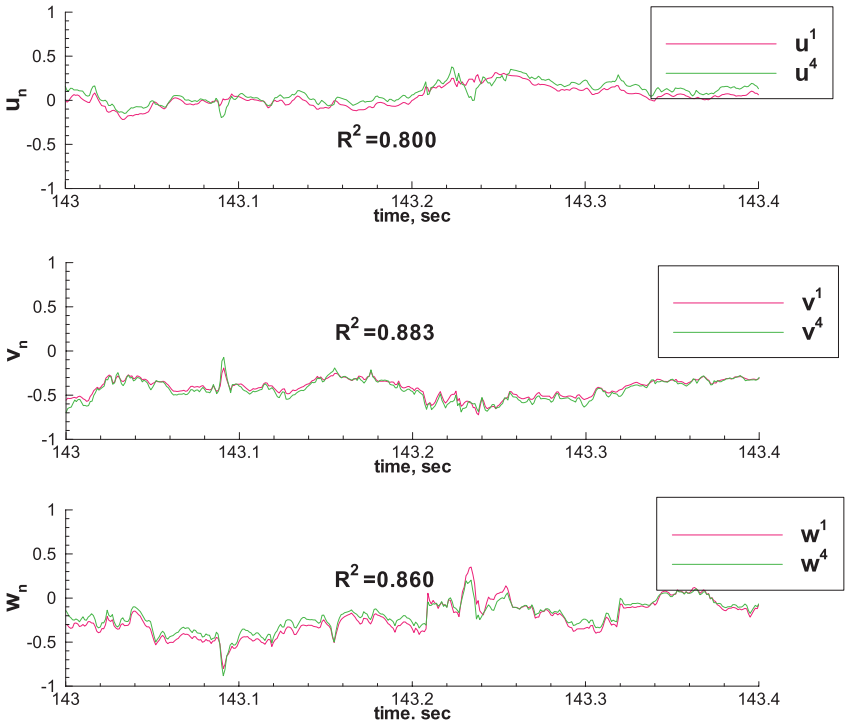

a)

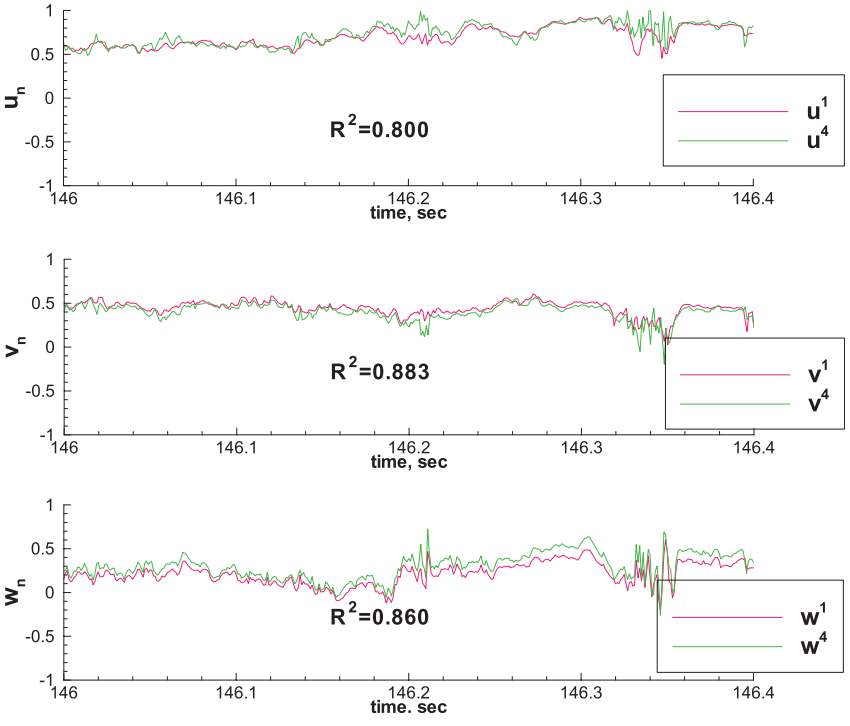

b)

FIG. 6. Two time-trace records for Field_Expt 1, midafternoon on 30 Mar 2008, with (a) reasonable agreement and (b) strong bursts: (top) streamwise, (middle) transverse, and (bottom) vertical normalized velocity component. Red plot shows CBS-PF, and green plot shows SBS-NN. For superscripts see Table 1. The start time in Fig. 6a is 1415 LT.

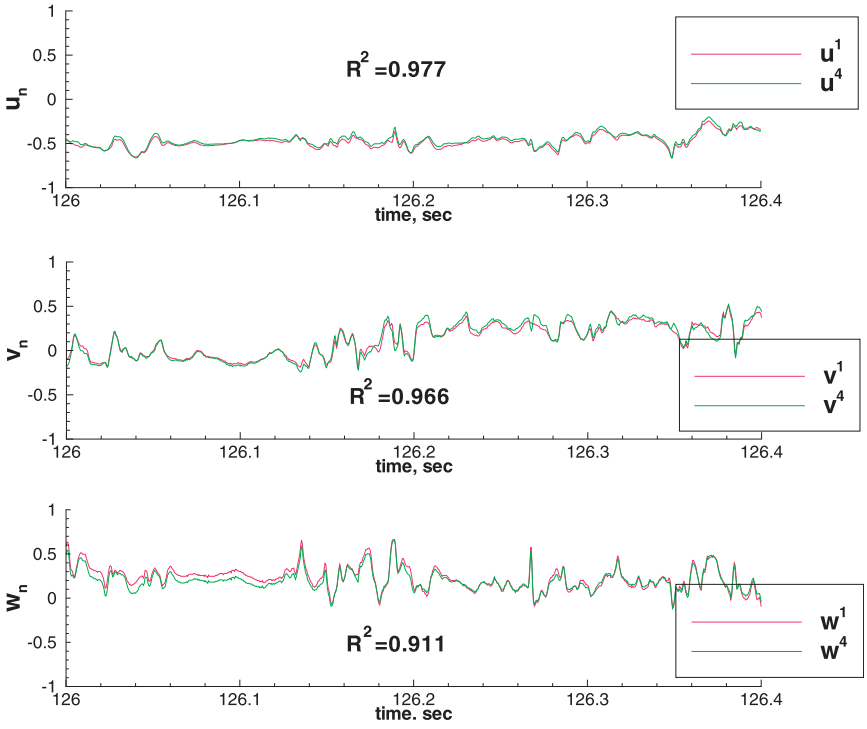

FIG. 7. As in Fig. 2, but for Field_Expt 2 nocturnal measurements on 5 Apr 2008, and green plot shows SBS-NN.

probes can provide such information, but they require frequent and laborious calibrations as well as specific alignments of probes with the flow. The latter problem was circumvented by designing a platform where the hot-film probes automatically adjust to the wind direction prompted by in situ information provided by the collocated sonic anemometer. To address the former problem, the possibility of using an NN for in situ

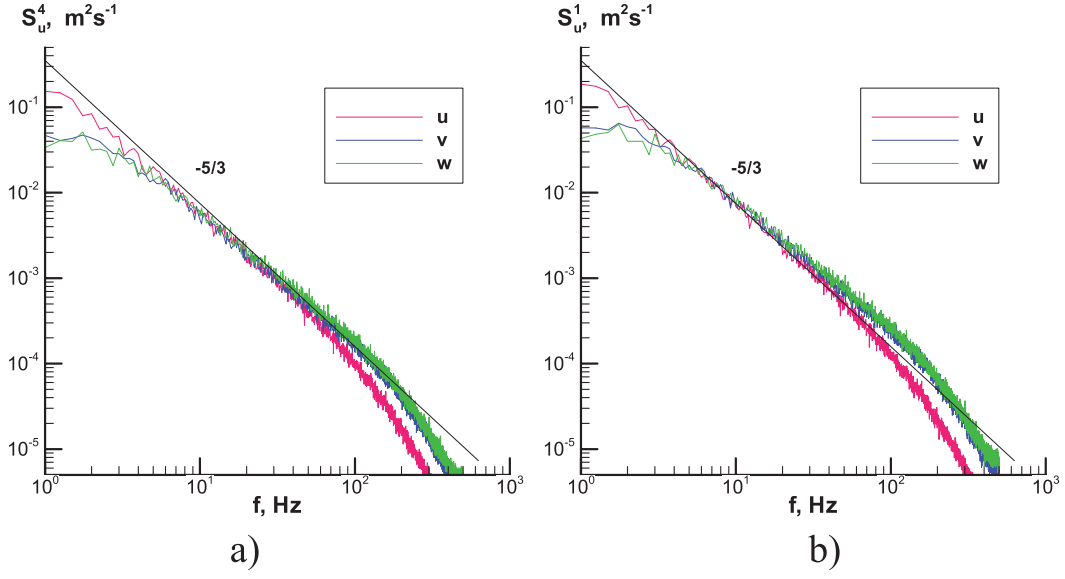

FIG. 8. Spectra of u (red), v (blue), and w (green) using (a) SBS-NN and (b) CBS-PF procedures for Lab_Expt 1. For superscripts see Table 1.

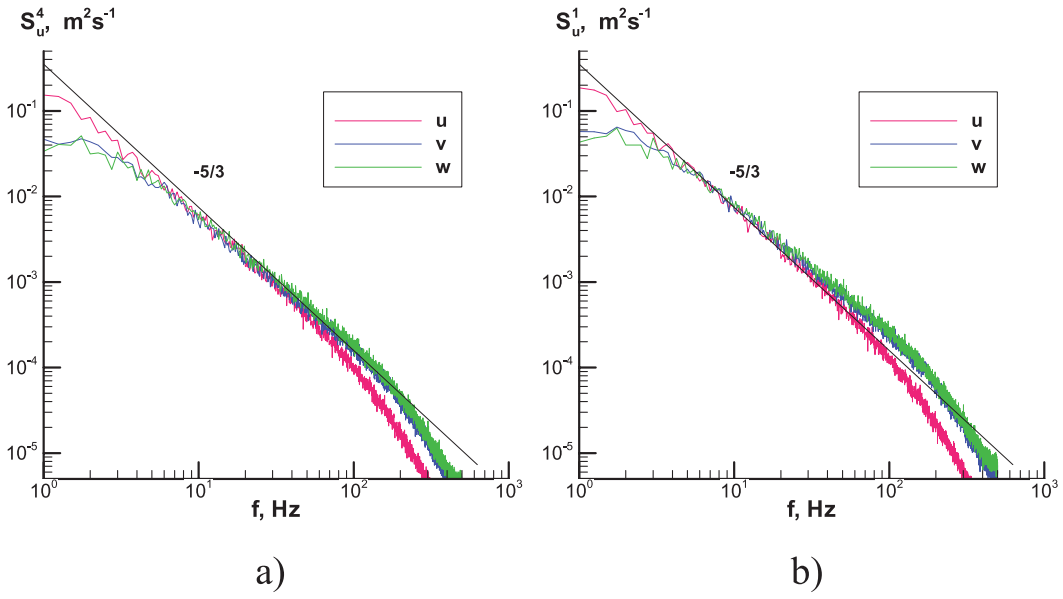

FIG. 9. As in Fig. 8, but for Lab_Expt 2.

calibration of hot films was studied. To this end, the hot-film velocity outputs based on the standard calibration method and the corresponding outputs from a calibration based on an NN were compared for both laboratory and atmospheric turbulent flows. The standard calibration was conducted using a known flow obtained in a low-turbulence jet facility or a calibrator, and polynomial fitting was used to obtain input–output relations. In the sonic-anemometer-based calibration, a collocated sonic was used to obtain the calibration velocity, and an NN was used to obtain the input–output relation.

The present work involved addressing some technical and logistical challenges. The velocity at the calibrator (the jet nozzle where turbulence level is negligible) and the yaw angle of the hot film were systematically changed to acquire data for 2D probe calibration. This method was acceptable, given that the total probe was an assemblage of two X hot films. During the calibration stage, they were oriented in the horizontal plane,

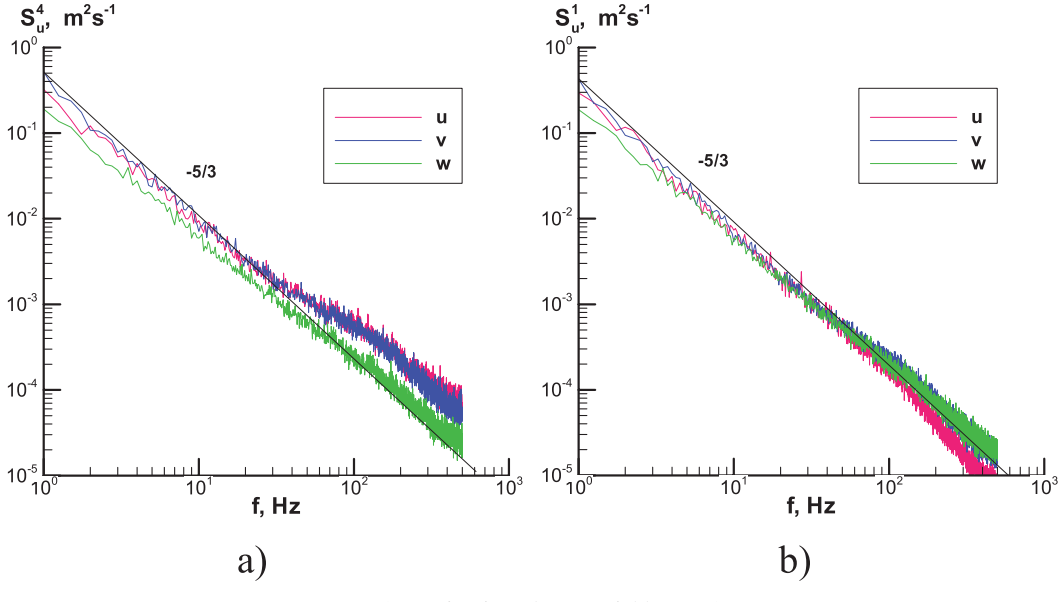

FIG. 10. As in Fig. 8, but for Field_Expt 1.

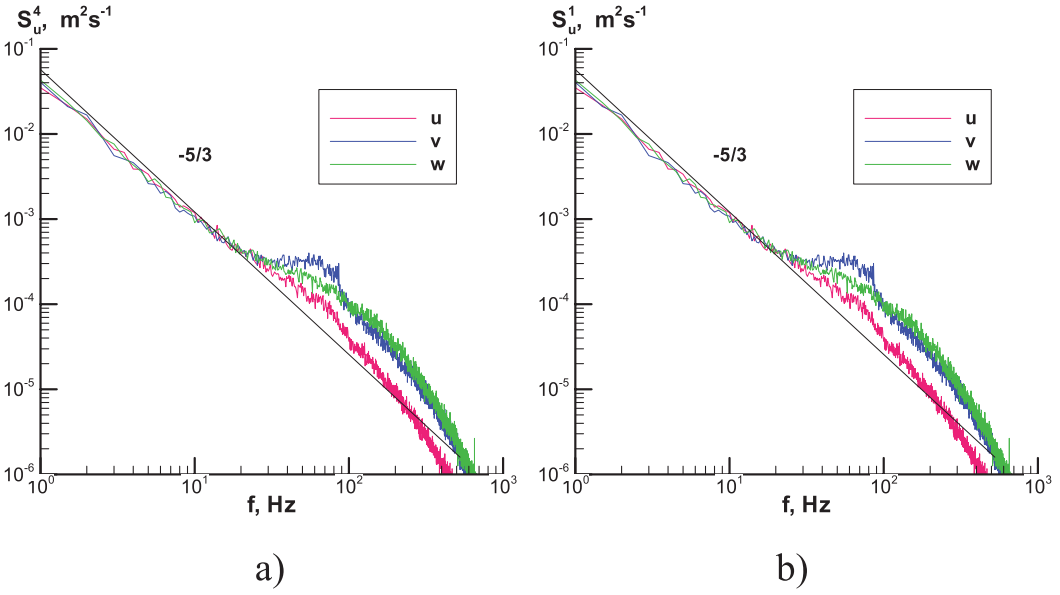

FIG. 11. As in Fig. 8, but for Field_Expt 2.

and one of the probes was then rotated so that the probe planes were mutually orthogonal, thus allowing the measurement of all three components. This is a commonly used procedure for a single X-hot-film probe (referred to as CBS), and for evenly distributed calibration datasets so obtained the direct polynomial least squares fit (PF) is an established method to approximate input–output relations (CBS-PF; also referred to as the standard calibration method). The same relationship was also obtained using NN (CBS-NN) and was found to be indistinguishable from CBS-PF for evenly distributed datasets.

The calibrated hot film was then collocated with the sonic to conduct measurements in the same jet but at a downstream distance where the flow is fully turbulent; with incremental changes of the jet mean velocity similar to those used in CBS (i.e., evenly spaced; however, the instantaneous velocities are random fluctuations superimposed on the mean). The new calibration dataset (SBS) comprises low-pass-filtered velocities and voltages measured by sonic and hot films, respectively, which was used to establish velocity/voltage calibration relation either by training an NN (SBS-NN) or using a PF (SBS-PF). Both were then employed to evaluate jet turbulence downstream of the nozzle, which could be compared with the velocity, obtained using the standard CBS-PF.

The instrument combination was then placed in the lower atmospheric boundary layer, and the standard jet-based CBS was obtained on location, followed by measurements under convective and stably stratified conditions. In situ sonic and hot-film measurements were used to obtain calibration relations SBS-NN and SBS-PF.

The main results of the experimental program are as follows:

(i) For the laboratory turbulent jet, instantaneous velocities obtained using SBS-NN and standard calibration method (CBS-PF) were almost similar,

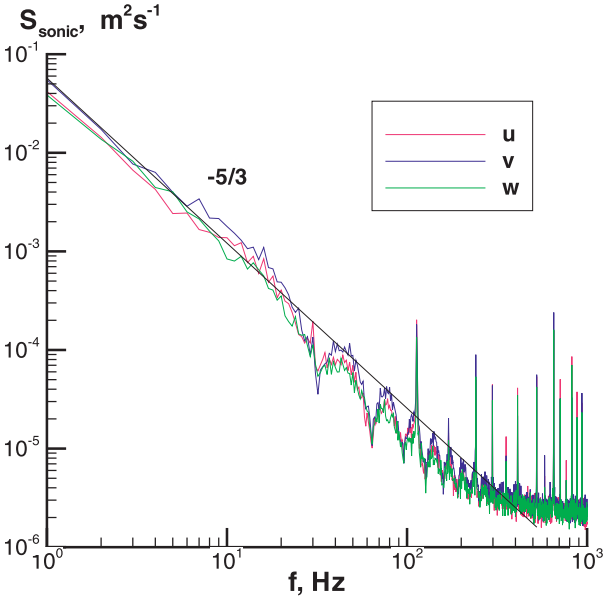

FIG. 12. Spectra of u (red), v (blue), and w (green) velocity data from sonic anemometer for Field_Expt 2.

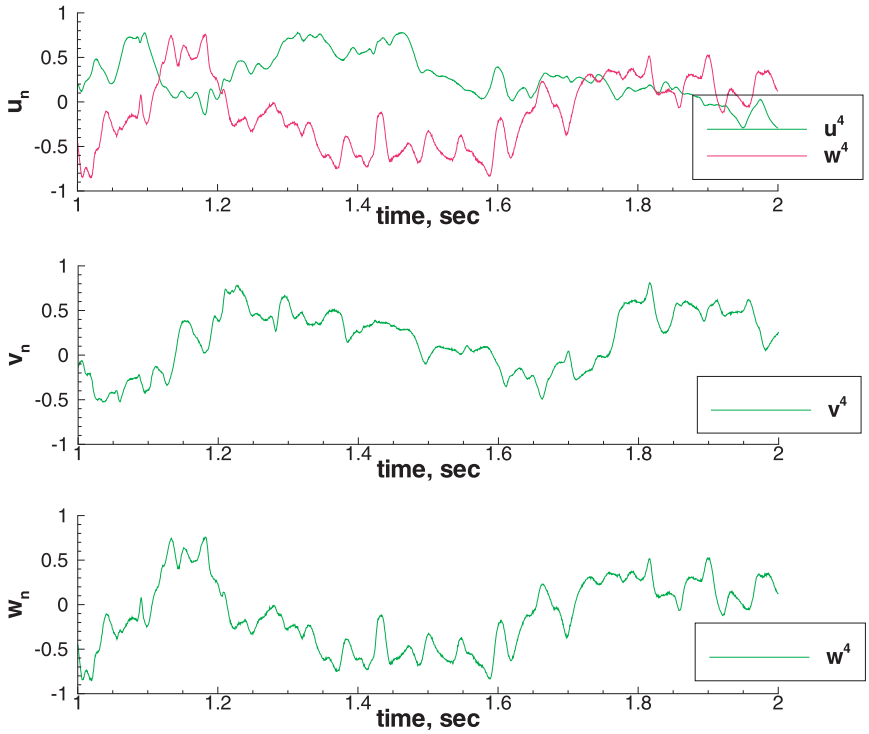

FIG. 13. Variation of normalized velocity components with time. Measurements by the NCAR group during night (T-REX experiment). For superscripts see Table 1.

indicating striking success of both methods in the laboratory and the possibility of replacing the (laborious) CBS-PF method using an SBS-NN. The SBS-PF method did not perform well against CBS-PF and is not recommended.

(ii) Under atmospheric field conditions as well, the agreement between data processed using SBS-NN and standard CBS-PF was acceptable when the flow is stably stratified (nocturnal boundary layer), whereas the agreement was unacceptable during convective conditions, particularly when thermal-burst-like motions are present. A possible reason is higher vertical velocities prevailing under burst conditions, which makes our standard calibration procedures inapplicable. More work is necessary with 3D probes and calibrations to resolve the issue. The SBS-PF was found to be highly unsatisfactory for hot-film calibration in the field.

In all, the NN technique offers great potential to be used in field calibrations of hot-film/sonic anemometer combinations, thus avoiding laborious repeated calibrations using an external calibrator such as a controlled jet used in our studies. At present, the use of SBS-NN technique can be confidently recommended for the in situ calibration of hot films for the case of atmospheric stable boundary layer.

Acknowledgments. This work is supported by the Bi-National Science Foundation (Grant 2004087) and in part by the Israel Science Foundation (Grant 964/05) and the U.S. National Science Foundation (ATM). The authors are grateful to Dr. Greg Poulos and his colleagues at NCAR for providing raw data, Professor I. Wygnanski for help in building the jet facility, and the Maricopa County Air Quality Division for allowing us to use one of their test sites.

TABLE 3. Mean, RMS, and correlation of voltages (E_1, E_2, E_3) across the wires of hot-film probe and velocity components (u, v, w).

	E_1 (V)	E_2 (V)	E_3 (V)	u (m s^{-1})	v (m s^{-1})	w (m s^{-1})
Mean	2.048	2.086	2.041	1.039	−0.0738	−0.0420
RMS	0.0323	0.0304	0.0335	0.0977	0.1294	0.0681
Correlation coefs	$\overline{E_1E_2}$	$\overline{E_1E_3}$	$\overline{E_3E_2}$	$\overline{uv}$	$\overline{uw}$	$\overline{wv}$
	0.6590	0.7406	0.8617	0.0305	−0.2331	0.0449

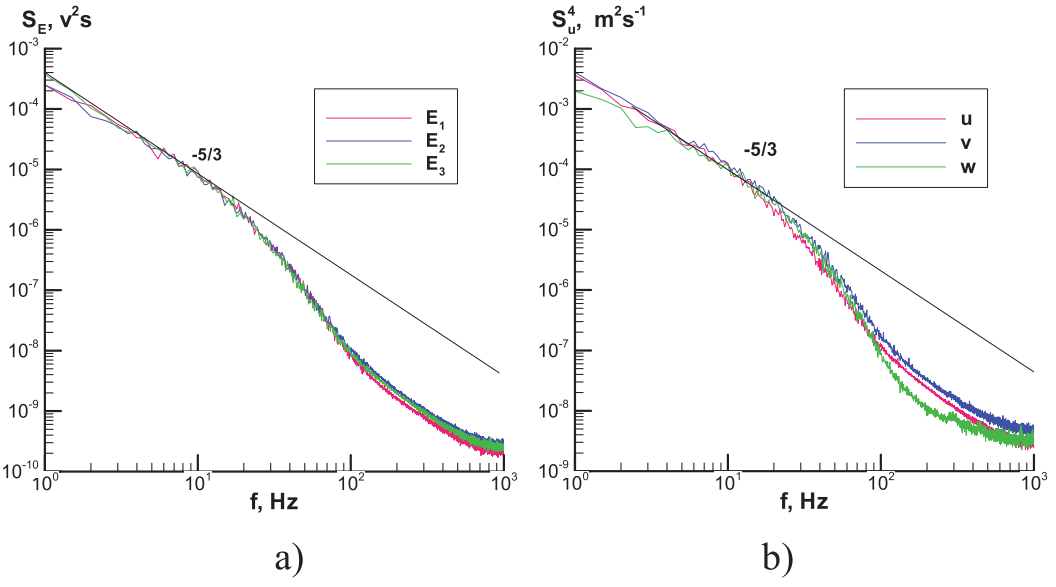

FIG. 14. Spectra of NCAR data from Fig. 13: (a) spectra of three voltages measured by triple-sensor hot-film and (b) spectra of velocities. For superscripts, see Table 1.

APPENDIX

Short Description of Neural Network Procedure

In the current work, the neural network procedure was based on the multilayer perceptron (MLP) approach. The model of the k neuron can be described as

$$u_k = \sum_{j=1}^{m} w_{kj} x_j \quad \text{and} \quad y_k = \varphi(u_k + b_k) = \varphi(v_k),$$

where x_j is the jth input signal at the kth neuron, $j = 1, 2, \ldots, m$; y_k is the output of the kth neuron; w_{kj} is the synaptic weights vector for the kth neuron; u_k is the linear combination of inputs; b_k is the activation

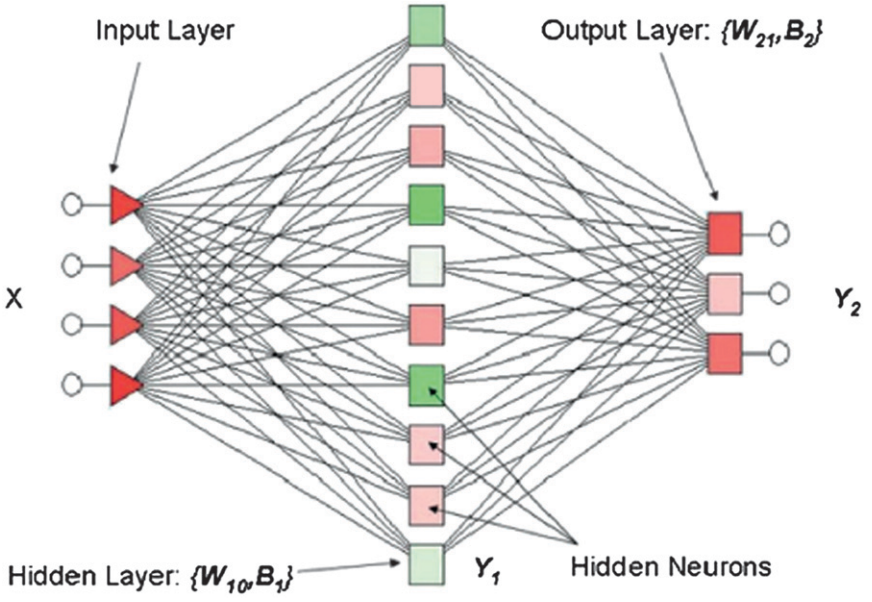

FIG. A1. The structure of the generated neural network.

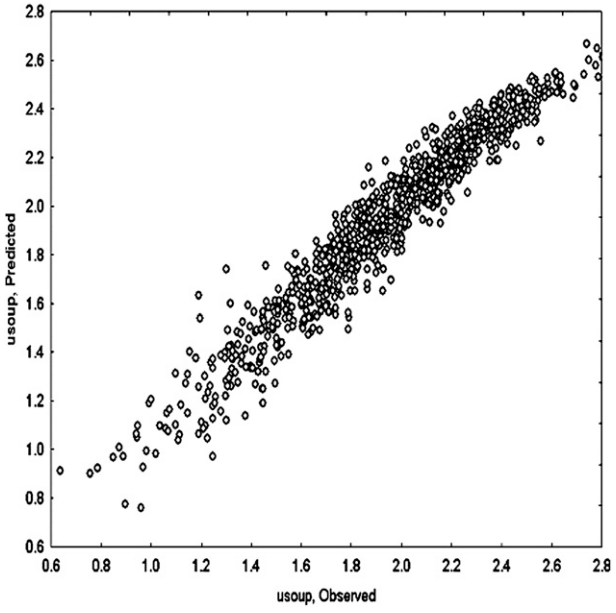

FIG. A2. The *u* scatterplot.

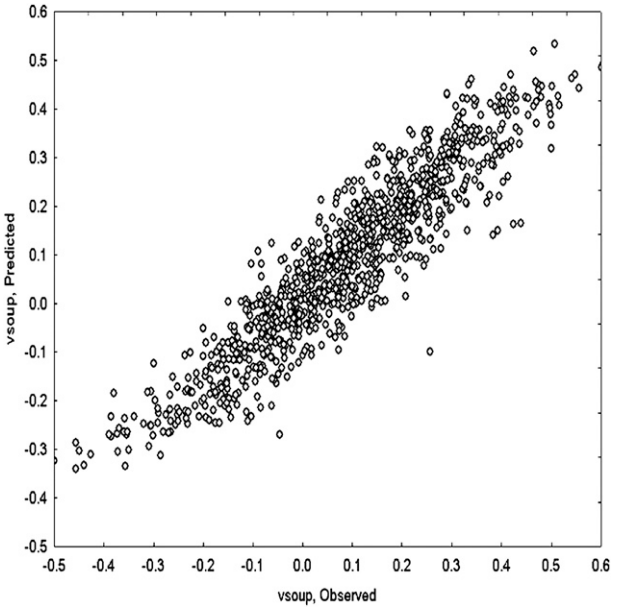

FIG. A3. The *v* scatterplot.

threshold of the *k*th neuron; v_k is the activation potential of the *k*th neuron; and φ is the activation function. The activation potential v_k is the inner product of the input vector $\mathbf{X}$ on the vector of the synaptic weights $\mathbf{W}$, which is biased relative to u_k by activation threshold b_k.

MLP contains one input layer, one or two hidden layers, and one output layer. The number of nodes of the input layer and the number of input signals are the same. We have used a fully connected network. In this case, each node of the input layer duplicates and sends its input signal to every neuron of the first hidden layer. The hidden layer consists of a number h of neurons. Each *k*th neuron transforms m input signals to its output y_k by applying this model, which is determined by the specific vector of synaptic weights w_{kj}, activation threshold b_k, and activation function φ. Then, this output is sent to every neuron of the second hidden layer or to the output layer. The number of neurons at the output layer is equal to the dimension of the neural networks output signal.

In our case, the calibration model represents a three-layer perceptron (MLP3) with input (zero) layer, one hidden (first) layer, and output (second) layer. The number of inputs of neural network is $m = 4$, the number of the hidden neurons is $h = 10$, and the number of the neurons at the output layer is $q = 3$. The structure of the generated fully connected neural network is shown in Fig. A1. The output $\mathbf{Y}_2$ of the MLP3 network can be represented as

$$\mathbf{Y}_2 = \varphi_2(\mathbf{Y}_1\mathbf{W}_{21} + \mathbf{B}_2) \quad \text{and}$$

$$\mathbf{Y}_1 = \varphi_1(\mathbf{X}\mathbf{W}_{10} + \mathbf{B}_1),$$

where $\mathbf{X}$ is the input of the network: $\dim\mathbf{X} = (1 \times 4)$, $\mathbf{Y}_1$ is the output of the hidden layer: $\dim\mathbf{Y}_1 = (1 \times 10)$, $\mathbf{Y}_2$ is the output of the network: $\dim\mathbf{Y}_2 = (1 \times 3)$, $\mathbf{W}_{10}$ is the matrix of synaptic weights for the hidden layer: $\dim\mathbf{W}_{10} = (4 \times 10)$, $\mathbf{W}_{21}$ is the matrix of synaptic weights for the output layer: $\dim\mathbf{W}_{21} = (10 \times 3)$, $\mathbf{B}_1$ and $\mathbf{B}_2$ are

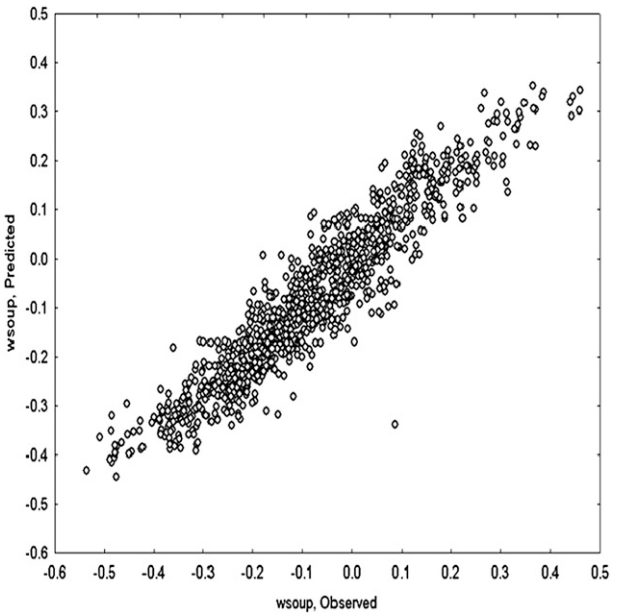

FIG. A4. The *w* scatterplot.

the vectors of activation threshold for the hidden and output layers, respectively, and φ_1 and φ_2 are the activation functions for the hidden and output layers, respectively. We have used hyperbolic tangent activation function $\varphi_1(v) = \tanh(v)$ for the hidden layer and logistic function $\varphi_2(v) = [1 + \exp(-v)]^{-1}$ for the output layer.

For the training of MLP, the back propagation and conjugate gradient descent methods were sequentially used. In all cases, the number of epochs that was necessary for the generation of the neural network did not exceed 100.

The matrix of activation functions and vectors of activation threshold for the hidden and output layers are shown here:

$$\mathbf{W}_{10} = \begin{bmatrix} -1.112 & -0.100 & 0.053 & -0.198 & 0.093 & 0.999 & -0.620 & -1.511 & -0.288 & -0.268 \\ 0.871 & -0.332 & 0.742 & 0.365 & -0.639 & -0.199 & 1.411 & 1.150 & -0.239 & 0.784 \\ 0.460 & -0.848 & 0.112 & -0.431 & 1.159 & -1.652 & -0.642 & -0.700 & -1.453 & 0.615 \\ -1.385 & 0.137 & -0.949 & 0.645 & -0.282 & 0.817 & 0.391 & 1.194 & 1.220 & -0.020 \end{bmatrix},$$

$$\mathbf{W}_{21} = \begin{bmatrix} -1.521 & 1.441 & -0.502 \\ -1.154 & -0.400 & 0.808 \\ 0.516 & 0.407 & -0.580 \\ -0.140 & 0.798 & 0.287 \\ 0.085 & -0.029 & -1.554 \\ -0.165 & -1.169 & 1.968 \\ 0.006 & 1.461 & 1.239 \\ 0.762 & 1.594 & 1.160 \\ -0.663 & -0.006 & 1.443 \\ 0.423 & 0.450 & -0.276 \end{bmatrix},$$

$$\mathbf{B}_1 = [-0.841 \quad -0.861 \quad -0.511 \quad 0.953 \quad 0.319 \quad -0.187 \quad 0.785 \quad -0.187 \quad -0.563 \quad 0.797], \text{ and}$$

$$\mathbf{B}_2 = [-0.199 \quad -0.389 \quad 0.296].$$

A typical example (Lab_Expt 1) yields the following correlation coefficients between the observed and the predicted values of outputs $r_u = 0.966$, $r_v = 0.926$, and $r_w = 0.943$. Scatterplots for the observed and predicted values of outputs in the training set are shown in Figs. A2–A4.

REFERENCES

Al-Salaymeh, A., and M. S. Ashhab, 2006: Modelling of a novel hot-wire thermal flow sensor with neural nets under different operating conditions. *Sens. Actuators,* **126A,** 7–14.

——, and ——, 2007: Modeling of the response of a hot-wire anemometer with neural nets under various air densities. *Sens. Transducers J.,* **84,** 1590–1606.

Ashhab, M. S., and A. Al-Salaymeh, 2006: Optimization of hot-wire thermal flow sensor based on a neural net model. *Appl. Therm. Eng.,* **26,** 948–955.

Balint, J.-L., P. Vukoslavcevic, and J. M. Wallace, 1987: A study of the vortical structure of the turbulent boundary layer. *Advances in Turbulence,* G. Compte-Bellot and J. Mathieu, Eds., Springer, 450–464.

——, ——, and ——, 1988: The transport of enstrophy in a turbulent boundary layer. *Near Wall Turbulence: 1988 Zoran Zaric Memorial Conference,* Dubrovnik, Croatia, 932–950.

——, J. M. Wallace, and P. Vukoslavcevic, 1991: The velocity and vorticity vector fields of a turbulent boundary layer. Part 2. Statistical properties. *J. Fluid Mech.,* **228,** 53–86.

Cornman, L. B., G. Meymaris, and M. Limber, 2004: An update on the FAA Aviation Weather Research Program's in situ turbulence measurement and reporting system. Preprints, *11th Conf. on Aviation, Range, and Aerospace Meteorology,* Hyannis, MA, Amer. Meteor. Soc., 4.3. [Available online at http://ams.confex.com/ams/pdfpapers/81622.pdf.]

Dobbeling, K., B. Lenze, and W. Leuckel, 1990: Basic considerations concerning the construction and usage of multiple hot-wire probes for highly turbulent three-dimensional flows. *Meas. Sci. Technol.,* **1,** 924–933.

——, ——, and ——, 1992: Four-sensor hot-wire probe measurements of the isothermal flow in a model combustion chamber at different levels of swirl. *Exp. Therm. Fluid Sci.,* **5,** 381–389.

Fang, M., J. Zhang, K. Williams, and J. A. Craig, 2008: Three-dimensional mosaic of the eddy dissipation rate fields from WSR-88Ds. Preprints, *13th Conf. on Aviation, Range and Aerospace Meteorology,* New Orleans, LA, Amer. Meteor. Soc., P4.5. [Available online at http://ams.confex.com/ams/pdfpapers/130591.pdf.]

Frehlich, R., and L. Cornman, 2002: Estimating spatial velocity statistics with coherent Doppler lidar. *J. Atmos. Oceanic Technol.,* **19,** 355–366.

Gulitski, G., M. Kholmyansky, W. Kinzelbach, B. Luthi, A. Tsinober, and S. Yorish, 2007a: Velocity and temperature derivatives in high-Reynolds-number turbulent flows in the atmospheric surface layer. Part 1. Facilities, methods and some general results. *J. Fluid Mech.,* **589,** 57–81.

——, ——, ——, ——, ——, and ——, 2007b: Velocity and temperature derivatives in high-Reynolds-number turbulent flows in the atmospheric surface layer. Part 2. Accelerations and related matters. *J. Fluid Mech.,* **589,** 83–102.

——, ——, ——, ——, ——, and ——, 2007c: Velocity and temperature derivatives in high-Reynolds-number turbulent flows in the atmospheric surface layer. Part 3. Temperature and joint statistics of temperature and velocity derivatives. *J. Fluid Mech.,* **589,** 103–123.

Haykin, S., 1998: *Neural Networks: A Comprehensive Foundation*. Prentice-Hall, 842 pp.

Hunt, J. C. R., 1984: Turbulence structure in thermal convection and shear-free boundary layers. *J. Fluid Mech.,* **138,** 161–184.

Jorgensen, F., 1971: Directional sensitivity of wire and fiber-film probes. *DISA Info,* **11,** 31–37.

Kaimal, J. C., and J. J. Finnigan, 1994: *Atmospheric Boundary Layer Flows: Their Structure and Measurement*. Oxford University Press, 289 pp.

Kit, E., A. Tsinober, J. L. Balint, J. M. Wallace, and E. Levich, 1987: An experimental study of helicity related properties of a turbulent flow past a grid. *Phys. Fluids,* **30,** 3323–3325.

——, ——, M. Teitel, J. L. Balint, J. M. Wallace, and E. Levich, 1988: Vorticity measurements in turbulent grid flows. *Fluid Dyn. Res.,* **3,** 289–294.

——, O. Krivonosova, D. Zhilenko, and D. Friedman, 2005: Reconstruction of large coherent structures from SPIV measurements in a forced turbulent mixing layer. *Exp. Fluids,* **39,** 761–770.

——, I. Wygnanski, O. Krivonosova, D. Zhilenko, and D. Friedman, 2007: On the periodically excited, plane turbulent mixing layer, emanating from a jagged partition. *J. Fluid Mech.,* **589,** 479–507.

Miller, D. R., J. Lin, Y. S. Wang, and H. W. Thistle, 1989: A triple-hot-film and wind octant combination probe for turbulent air flow measurements in and near plant canopies. *Agric. For. Meteor.,* **44,** 353–368.

Monin, A., and A. Yaglom, 1971: *Statistical Fluid Mechanics: Mechanics of Turbulence*. Vol. 2, Dover, 782 pp.

Monti, P., H. J. S. Fernando, W. C. Chan, M. Princevac, T. A. Kowalewski, and E. Pardyjak, 2002: Observations of flow and turbulence in the nocturnal boundary layer over a slope. *J. Atmos. Sci.,* **59,** 2513–2534.

Nguyen, H. T., R. P. Nadipuram, C. L. Walker, and E. A. Walker, 2003: *A First Course in Fuzzy and Neural Control*. Chapman & Hall/CRC Press, 301 pp.

Pardyjak, E. R., P. Monti, and H. J. S. Fernando, 2002: Flux Richardson number measurements in stable atmospheric shear flows. *J. Fluid Mech.,* **449,** 307–316.

Poulos, G. S., S. Semmer, J. Militzer, and G. Maclean, 2006: A novel method for the study of near-surface turbulence using 3-d hot-film anemometry: OTIHS. Preprints, *17th Symp. on Boundary Layers and Turbulence,* San Diego, CA, Amer. Meteor. Soc., P2.3.

R. M. Young Company, 2001: Model 81000 ultrasonic anemometer. R. M. Young Manual PN 81000-90 REV 5-03A, 6 pp.

Skelly, B. T., D. R. Miller, and T. H. Meyer, 2002: Triple-hot-film anemometer performance in CASES-99 and a comparison to sonic anemometer measurements. *Bound.-Layer Meteor.,* **105,** 275–304.

Tsinober, A., E. Kit, and T. Dracos, 1992: Experimental investigation of the field of velocity gradients in turbulent flows. *J. Fluid Mech.,* **242,** 169–192.

van Dijk, A., and F. T. M. Nieuwstadt, 2004a: The calibration of (multi-) hot-wire probes. 1. Temperature calibration. *Exp. Fluids,* **36,** 540–549.

——, and ——, 2004b: The calibration of (multi-) hot-wire probes. 2. Velocity calibration. *Exp. Fluids,* **36,** 550–564.